F. Méot DAPNIA SACM

FFAG video conf., March 04

Tracking in FFAG magnets and rings using the ray-tracing code Zgoubi

Abstract

1 Introduction

The study is based on ray-tracing methods, using Zgoubi. The Zgoubi method is based on resolution of the equation of motion by means of Taylor expansion of particle position and velocity ; principles relevant to the present study are recalled in App. A, details can be found in Ref. [2].

2 Magnet simulation

The magnetic field along a particle trajectory, while nulerical integration of the Lorentz equation precedes, is calculated from the magnet geometry, which in turns involves the particular description of each one of the N separate dipoles that constitute the FFAG N-uplet, so as to allow field superposition within the all extent of the N-uplet.

2.1 Magnet geometry

The description of the geometry of the dipoles in an N-dipole FFAG has been adapted from the sophisticated "DIPOLE" procedure in Zgoubi[1] (this is addressed in App. B). This procedure allows EFB shaping, as shown on Fig. 1 : *EFB*s can be inclined, partly or fully curved, the angular opening (the β_F, β_D angles in the notations of Ref. [1, Chapter 2.2.4]) is arbitrary, entrance, exit and possibly lateral fringe field fall offs with arbitrary shapes can be accounted for (App. B).

The principle geometry of a FFAG triplet assembly based on what precedes is shown in Fig. 2.

[1] "DIPOLE" has been abundantly used for the purpose of large acceptance spectrometer design [3, *e.g.*], it can be considered to be one stage upstream of the use of magneitc field maps, because it allows fast adjustment of the dipole geometric parameters, possibly automatically using the matching proceudre "FIT" in Zgoubi.

The 'DIPOLE' procedure. Design parameters of the SPS2 large acceptance spectrometer (see also, e.g., SPEG at GANIL, QD KAON at GSI).

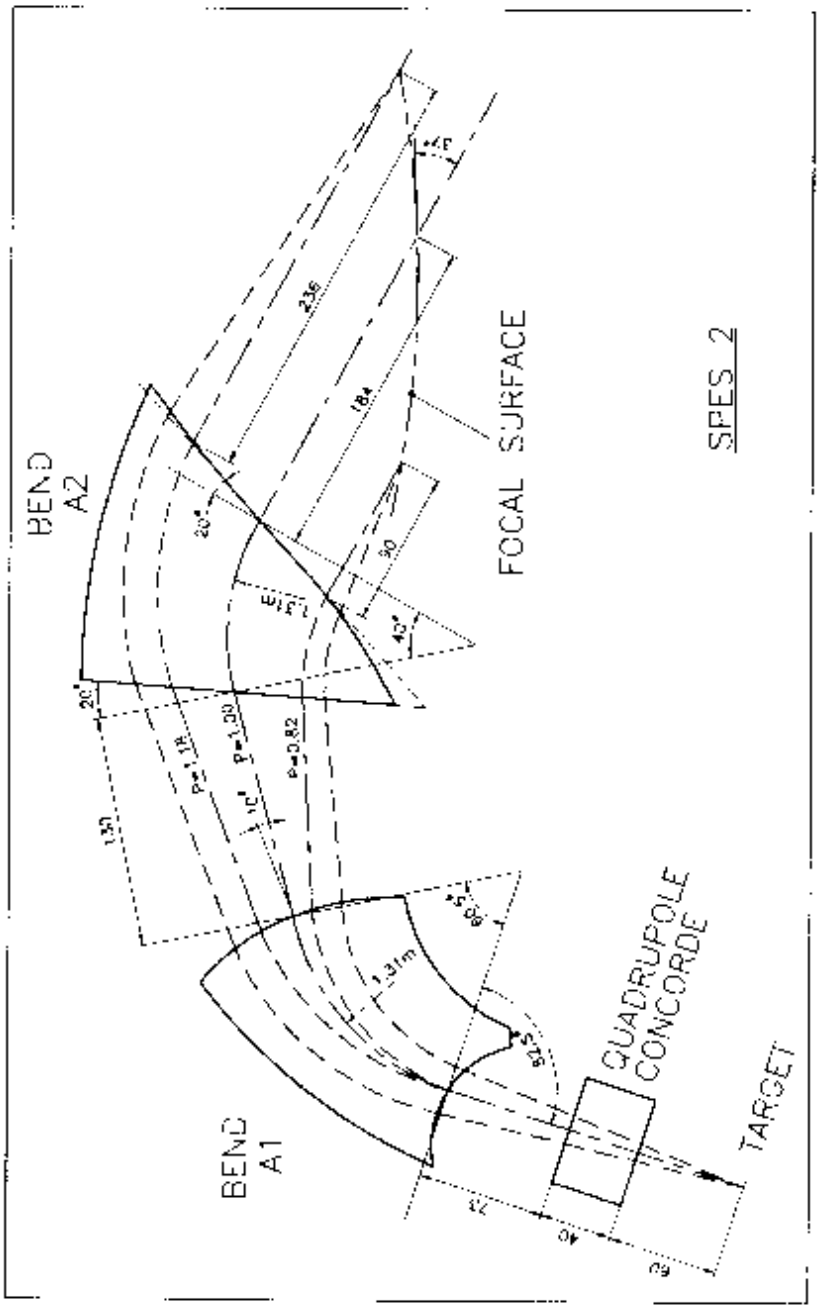

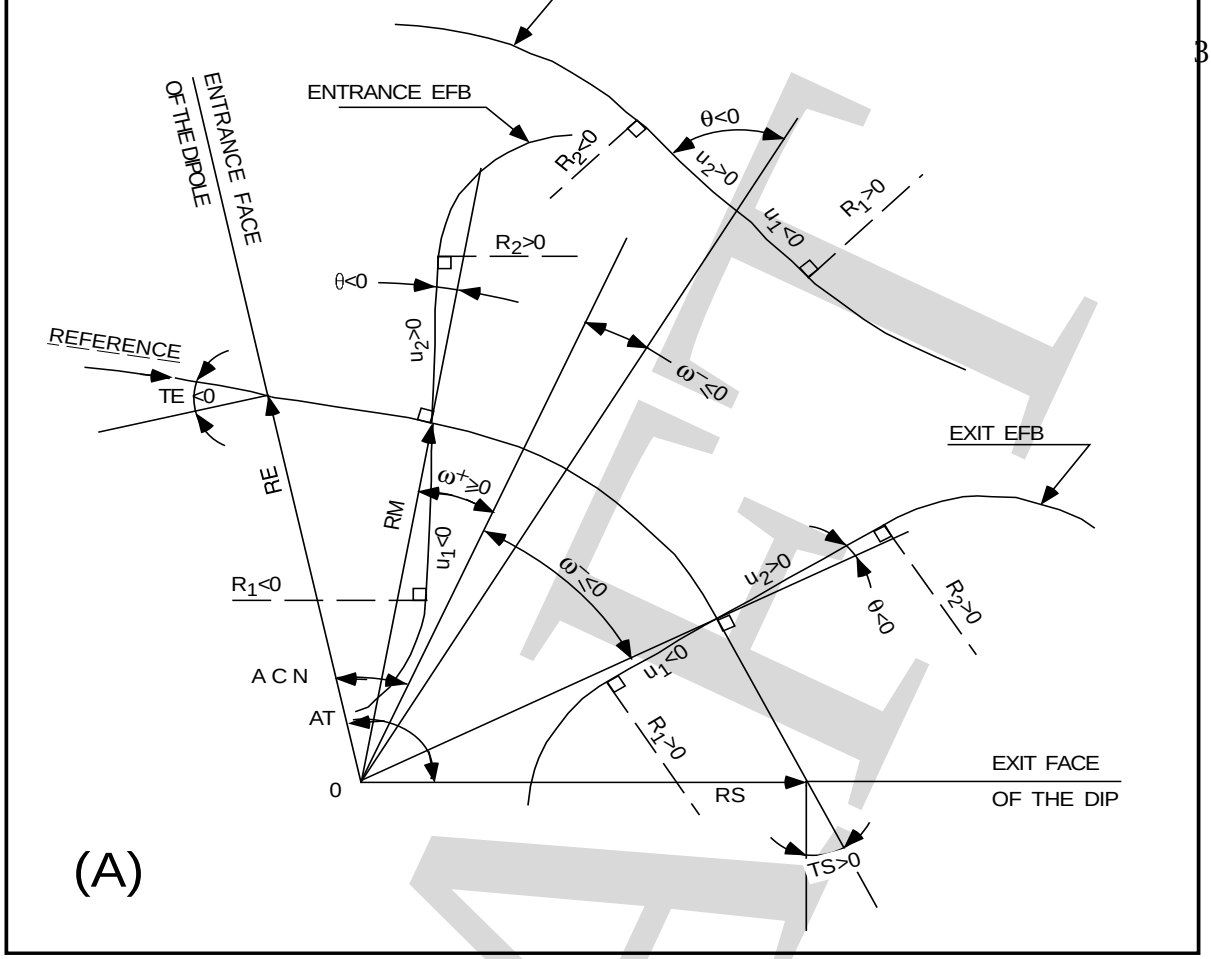

Figure 1: Description of the geometry of a single dipole. A reference radius RM and a reference angle ACN serve for the positionning of the entrance, exit and possibly lateral EFBs. These can be curved, tilted, etc. The total angular aperture AT of the field extent accounts for fringe field extent regions at both ends.

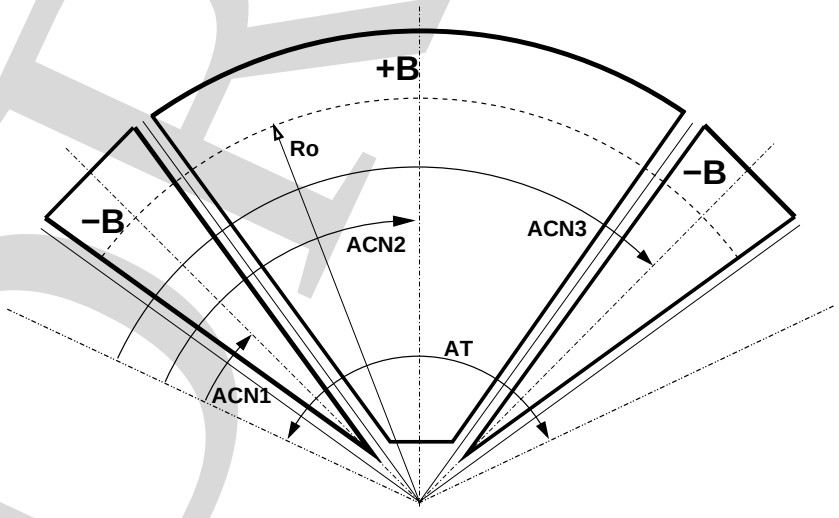

Figure 2: Principle scheme and description of an FFAG DFD triplet. The three sectors are positionned in the triplet frame by means of the three angles ACN_{1-3}. The average radius RM in Fig. 1 takes the particular value R_0 (Eq. 3). Compared to the sophisticated possibilities shown in Fig. 1 the sector dipoles of the FFAG magnet are much simpler : no wedge angle, straight EFBs, etc.

2.2 Overlapping of fringe fields

The overlapping of fringe fields in an FFAG magnet as due to the neighboring ends of its constitutive dipoles is treated by applying the principle of superposition in the manner described in App. B. Results so obtained for the simulation of the FFAG triplet (Fig. 2) in J-NuFact first muon ring are displayed in Fig. 3.

The superposition of the three separate contributions insures a continuous fall-off factor over the all extent of the FFAG magnet assembly. The extrapolation off median plane (the $z = 8$ cm case in Fig. 3) yields correct field behavior. Such results are liable to yield precision tracking.

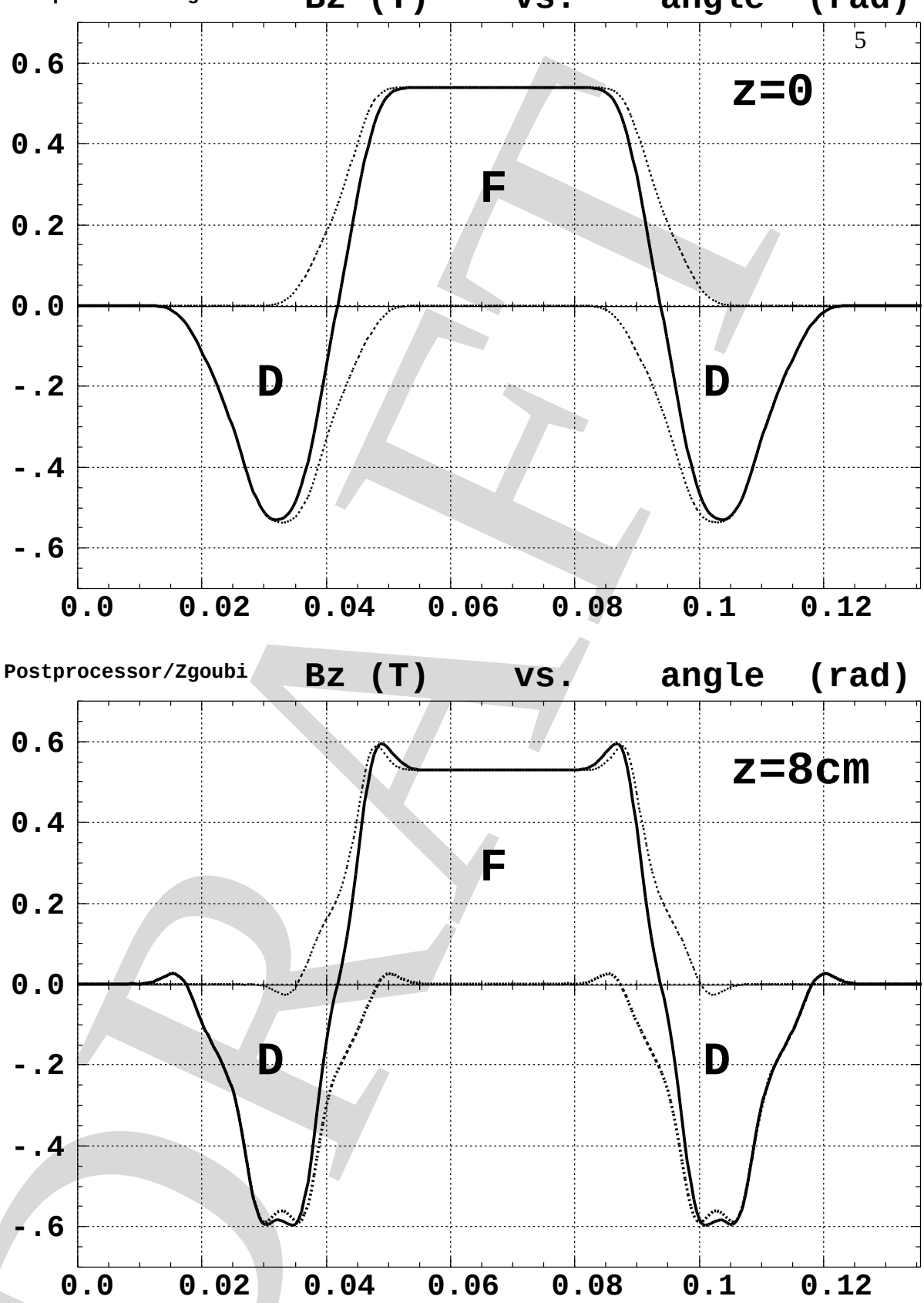

Figure 3: Typical magnetic field, as observed at traversal of the $K = 50$ FFAG triplet for $r = 20.52$ m and for either $z = 0$ or $z = 8$ cm. On both plots the solid curve represents the effective field, as obtained by superposition of the separate contributions of each one of the three dipoles represented by the dashed curves.

3 Particle motion

3.1 First order data

The reference closed orbit, tunes, etc. can be drawn from multiturn tracking

```
Beam  matrix  (beta/-alpha/-alpha/gamma) and  periodic  dispersion  (MKSA units

   Ri1           Ri2          Ri3          Ri4          Ri6
 3.820778     0.000002                                0.775893
 0.000002     0.261727                                0.000001
                          15.068870     0.000013
                           0.000013     0.066362

       Betatron  tunes :

       NU_Y = 0.14369817
       NU_Z = 0.41756588E-01
```

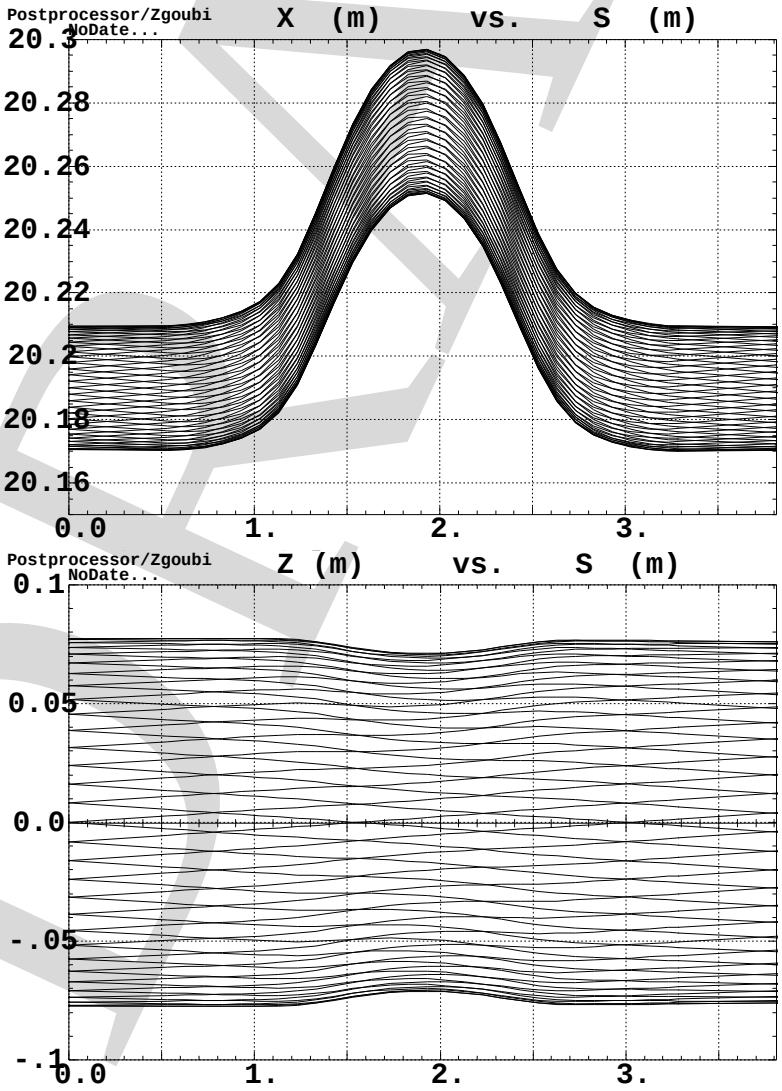

Figure 4: Beam tubes in a cell, radial (X) and vertical (Z).

3.2 Transverse phase space

Results in Figs. 5, 6. The vertical motion can be tracked to very large excursions, more than 3 cm emittance, no spiral effect, etc.

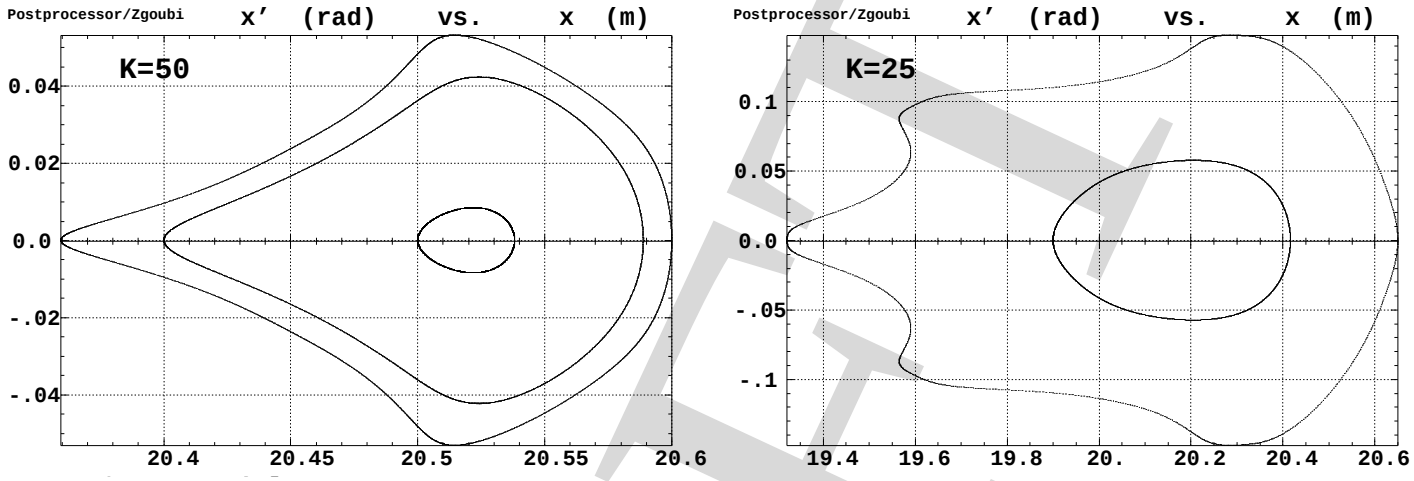

Figure 5: Horizontal phase space motion for particles launched in the horizontal plane, about 6000 pass performed in a single cell, equivalent to 200 turns in the 32 cells ring. Left plot : $K = 50$ triplet, $r = 20.4,\ 20.5$ and 20.6 m ; right plot : $K = 25$ triplet, $r = 19.9$ and 20.65 m.

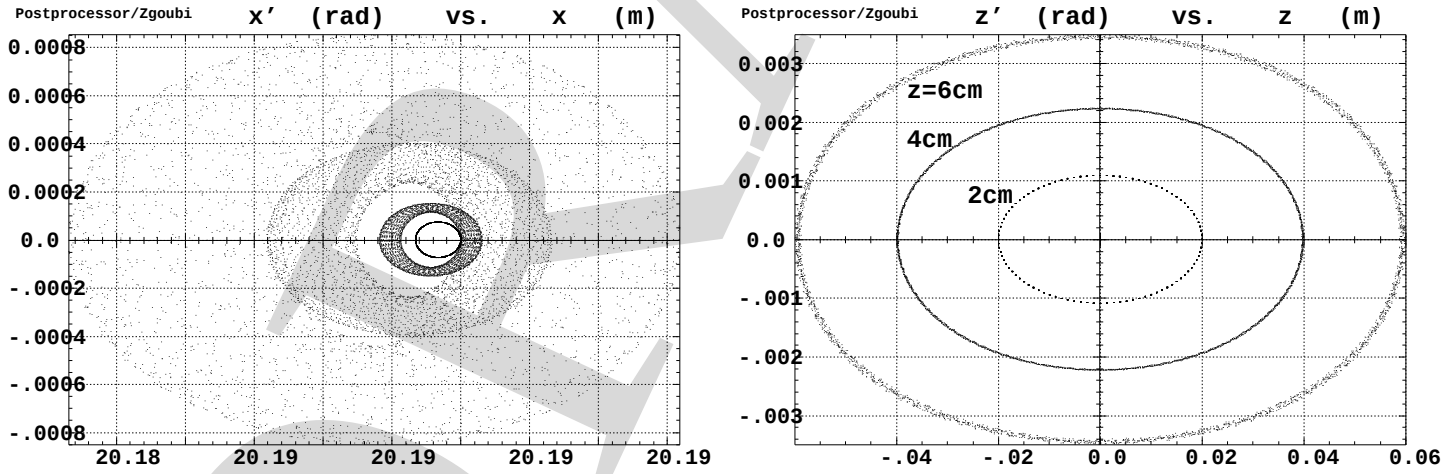

Figure 6: Horizontal (left) and vertical (right) phase spaces for 4 particles all launched with $r = 20.19$ m (i.e., vicinity of the horizontal closed orbit), and with respectively $z = 0,\ 2,\ 4, 6$ cm. 32000 pass in a single cell, equivalent to 1000 turns in the 32 cells ring. $K = 25$ FFAG triplet.

3.3 More optics

Closed orbits. Tunes : Fig. 8.

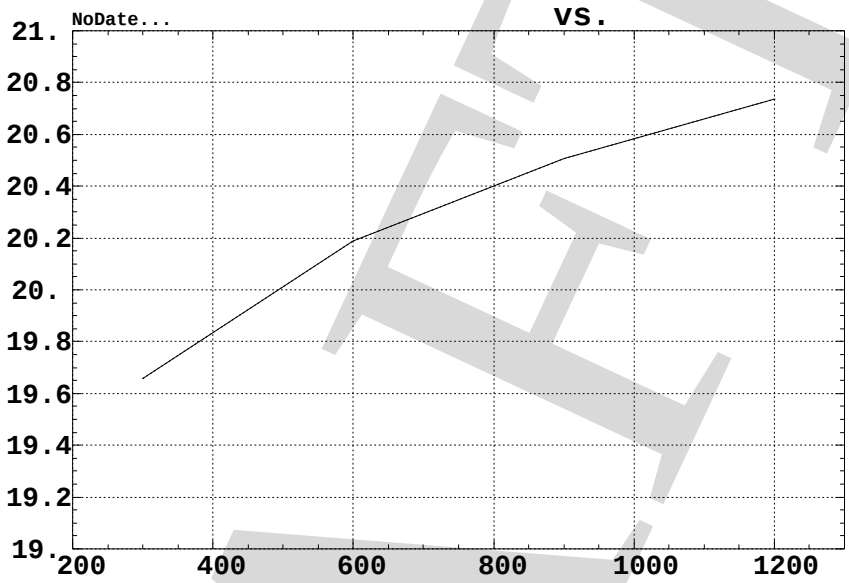

Figure 7: Closed orbit vs. momentum.

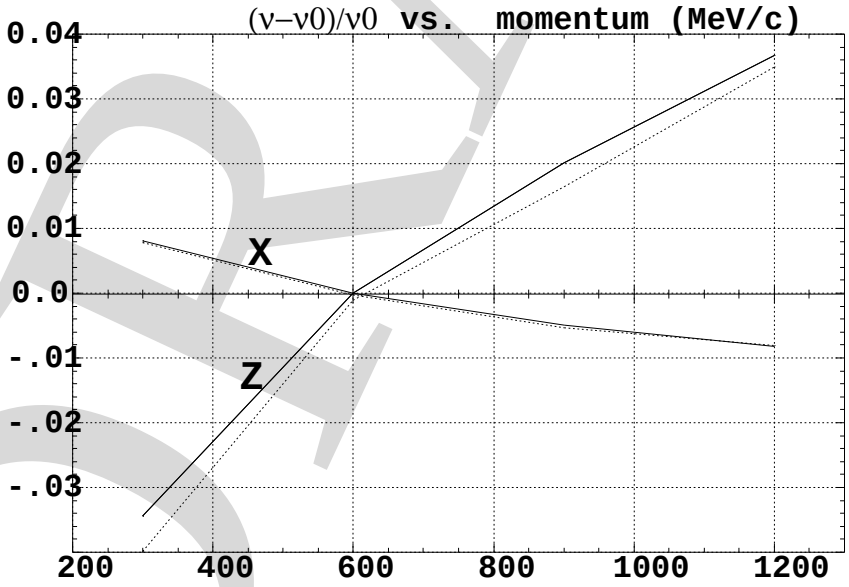

Figure 8: $(\nu - \nu_{600})\nu_{600}/$ vs. momentum, with $\nu_{x,600} = 0.1831$, $\nu_{z,600} = 0.0051$.

Conclusions

It would be interesting to compare the magnetic fields so obtained with 3-D magnet calculations.

The free access to alll the geometrical parameters that define the FFAG triplet allows optimisation by automatic matching methods (such as the ’FIT’ procedure in Zgoubi).

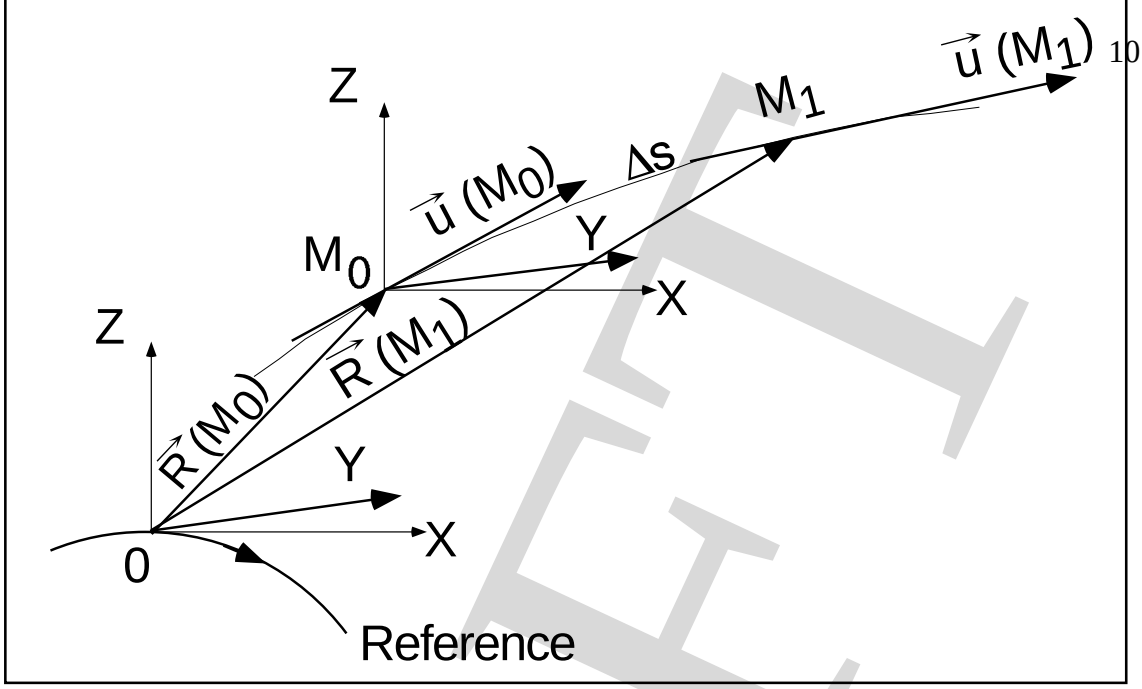

Figure 9: Zgoubi frame and coordinates.

APPENDIX

A On the ray-tracing method

The Zgoubi integration method is based on stepwise resolution of Lorentz equation by a technique of Taylor series, as descibed below.

Position and velocity

Position and velocity of a particle subject to $d(m\vec{v})/dt = q\,(\vec{e} + \vec{v}\times\vec{b})$ are tracked using truncated Taylor expansions

$$\begin{aligned} \vec{R}(M_1) &\approx \vec{R}(M_0) + \vec{u}(M_0)\,\Delta s + \vec{u}'(M_0)\,\tfrac{\Delta s^2}{2!} + ... + \vec{u}''''(M_0)\,\tfrac{\Delta s^6}{6!} \\ \vec{u}(M_1) &\approx \vec{u}(M_0) + \vec{u}'(M_0)\,\Delta s + \vec{u}''(M_0)\,\tfrac{\Delta s^2}{2!} + ... + \vec{u}''''(M_0)\,\tfrac{\Delta s^5}{5!} \end{aligned} \qquad (1)$$

wherein $\vec{u} = \vec{v}/v,\ \Delta s = v\,\Delta t,\ \vec{u}' = d\vec{u}/ds,\ m\vec{v} = mv\vec{u} = q\,B\rho\,\vec{u}$, and with the derivatives $\vec{u}^{(n)} = d^n\vec{u}/ds^n$ given by $\vec{u}' = \vec{u}\times\vec{B},\ \vec{u}'' = \vec{u}'\times\vec{B} + \vec{u}\times\vec{B}',\ \vec{u}''' = \vec{u}''\times\vec{B} + 2\vec{u}'\times\vec{B}' + \vec{u}\times\vec{B}''$, etc.

Taylor coefficients

The calculation of the coefficients in Eqs. 1 requires the knowledge of the magnetic field and derivatives, namely

$$\vec{B}(s), \qquad d^n\vec{B}/ds^n$$

in the cartesian frame (O,X,Y,Z) (Fig. 9).

On the other hand, the magnetic field in a dipole of an FFAG magnet is obtained from a median plane model in cylindrical coordinates, of the form $\mathcal{F}(r,\theta)B_0(r/R_0)^K$ (the factor $\mathcal{F}(r,\theta)$ accounts for field fall-offs at dipoles' ends). The way the field and its derivatives

$$B(r,\theta), \qquad \frac{\partial^{i+j}B}{\partial\theta^i\partial r^j} \tag{2}$$

at all (r,θ) in the FFAG magnet mid-plane are obtained from this model is detailed in App. B.

Once this is done, a transformation from the FFAG magnet cylindrical frame into Zgoubi cartesian frame is performed using

$$\frac{\partial B}{\partial X} = \frac{1}{r}\frac{\partial B}{\partial\theta},\ \frac{\partial B}{\partial Y} = \frac{\partial B}{\partial r},\ \frac{\partial^2 B}{\partial X^2} = \frac{1}{r^2}\frac{\partial^2 B}{\partial\theta^2} + \frac{1}{r}\frac{\partial B}{\partial r},\ \frac{\partial^2 B}{\partial X\partial Y} = \frac{1}{r}\frac{\partial^2 B}{\partial\theta\partial r} - \frac{1}{r^2}\frac{\partial B}{\partial\theta},\ \text{etc.}$$

Next, extrapolation off the median plane is obtained by Taylor expansions accounting for Maxwell equations, thus yielding

$$\vec{B}(X,Y,Z), \qquad \frac{\partial^{i+j+k}\vec{B}}{\partial X^i\partial Y^j\partial Z^k}$$

Eventually, $\vec{B}(s)$ and the $d^n\vec{B}/ds^n$ as needed in Eqs. 1 are derived from the above using the transformations

$$\vec{B}' = \sum_i \frac{\partial\vec{B}}{\partial X_i}u_i\,, \quad \vec{B}'' = \sum_{ij}\frac{\partial^2\vec{B}}{\partial X_i\partial X_j}u_iu_j + \sum_i\frac{\partial\vec{B}}{\partial X_i}u_i'\,, \qquad etc.$$

(wherein the $X_{i,j,...},\ i,j,... = 1,3$ stand for $X,\ Y$ or Z).

B An "FFAG" procedure

This Section describes the way the magnetic field and derivatives at all position (r, θ) in the median plane of an FFAG magnet are calculated in order to provide the ingredients necessary in Eqs. 1 as addressed in the previous Section.

The magnetic field at all (r, θ) in the median plane in a dipole (i) of a N-uplet FFAG magnet is given by

$$B_i(r, \theta) = \mathcal{F}_i(r, \theta) B_0 (r/R_0)^K \tag{3}$$

wherein the factor $\mathcal{F}_i(r, \theta)$ accounts for field fall-offs due to the dipoles' EFBs.

Field fall-offs

Field fall-offs due to magnet ends are modeled by [4, page 240]

$$\mathcal{F}_E = 1 + \exp[P(d)], P(d) = C_0 + C_1 \frac{d}{\lambda} + C_2 \left(\frac{d}{\lambda}\right)^2 + ... + C_5 \left(\frac{d}{\lambda}\right)^5 \tag{4}$$

wherein the index E stands for the EFB of concern, d is the distance to that EFB and depends on r and θ. The numerical coefficients λ, $C_0 - C_5$ can be determined from prior matching with numerical fringe field data. One can vary λ to possibly change or test the effect of the fall-off gradient, without affecting the position of the EFB (i.e., without any

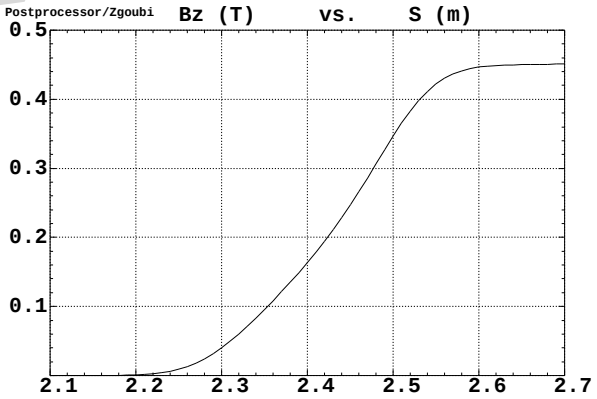

Figure 10: Fringe field as a function of distance.

effect on the effective magnetic length from entrance to exit EFB). However, moving EFBs is made possible through an independent parameter in the Zgoubi FFAG data list, “EFBS” (App. C).

Values used in the present study are

$$\lambda = 15,\ C_0 = 0.1455,\ C_1 = 2.2670,\ C_2 = -0.6395,\ C_3 = 1.1558,\ C_4 = C_5 =$$

and yield the fringe field shape shown in Fig. 10.

Considering that up to three EFBs intervene in the geometry of a dipole (Fig. 1) with each EFB its respective fringe field coefficient, $\mathcal{F}_{\text{Entrance}}$, $\mathcal{F}_{\text{Exit}}$, $\mathcal{F}_{\text{Lateral}}$, thus the resulting form factor at particle position due to dipole (i) of the N-uplet is taken to be

$$\mathcal{F}_i = \mathcal{F}_{\text{Entrance}} \times \mathcal{F}_{\text{Exit}} \times \mathcal{F}_{\text{Lateral}}$$

Superpositon

In the case of the N neighboring dipoles in an FFAG N-uplet, the total field at particle position is obtained by addition of the contributions of all dipoles, namely

$$B(r,\theta) = \sum_{i=1,N} B_i(r,\theta) \tag{5}$$

Field derivatives

As seen in Section A, at a particular stage in the stepwise integration procedure the field derivatives in the median plane are needed (Eq. 2). These are calculated numerically in the following way.

Eq. 5 is in fact used to get the magnetic field $B(r,\theta)$ at the $n * n$ nodes of a “flying” interpolation grid in the median plane

centered on the actual particle position as schemed in Fig. 11 ($n = 3$ or 5 in practice). A polynomial interpolation is involved, of the form

$$B(r,\theta) = A_{00} + A_{10}\theta + A_{01}r + A_{20}\theta^2 + A_{11}\theta r + A_{02}r^2$$

that yields the requested derivatives following

$$A_{kl} = \frac{1}{k!l!}\frac{\partial^{k+l}B}{\partial\theta^k\partial r^l}$$

Note that, the source code contains the explicit analytical expressions of the coefficients A_{kl} solutions of the normal equations, so that the operation is not particularly CPU time consuming.

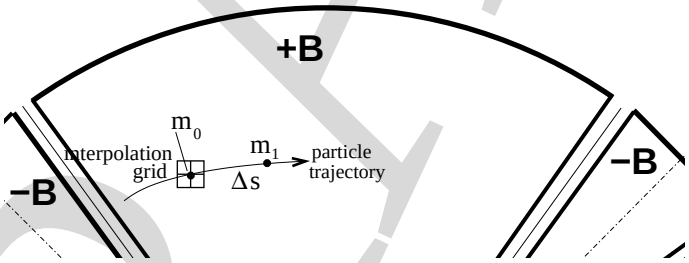

Figure 11: Principle scheme of the interpolation method used for calculation of the field derivatives in the median plane. m_0 and m_1 are the projections in the median plane of two successive particle positions M_0 and M_1 separated by one integration step Δs (Fig. 9).

C Zgoubi data file

Sample Zgoubi data of an FFAG cell.

```
FFAG triplet NuFact 0.3-1GeV
 'OBJET'
 1.98928E3                                                  beam rigidity (kG.cm)
 2
 3  1
2060 0. 0. 0. 0. 1.  'z'                                    initial coordinates of 3 particles
2050 0. 0. 0. 0. 1.  'z'
2040 0. 0. 0. 0. 1.  'z'
1 1 1
'FAISTORE'                                                  multiturn particle data storage
b_zgoubi.fai
1
 'DRIFT'
 156.
 'FFAG'
 0
 3   7.76988      2100.                                     number of dipoles, AT=tetaF+2tetaD+2Atan(XFF/R0), R0
 1.87959   0.  -18.  50. 0. 0.                             DIPOLE #1 : ACN1, unused, B0, K, unused
 15. -1.                                                      entrance EFB and fringe field : lambda, flag
 4  .1455   2.2670  -.6395  1.1558  0. 0.  0.                  # of non-zero C_i,  C_i (i=0,5), EFBS
 0.5156620156177409   0.    1.E6  -1.E6  1.E6  1.E6
 15. -1.                                                      exit EFB : lambda, flag
 4  .1455   2.2670  -.6395  1.1558  0. 0.  0.                  # of non-zero C_i,  C_i (i=0,5), EFBS
-0.5156620156177409   0.    1.E6  -1.E6  1.E6  1.E6
 0. 0.
 0  0.      0.      0.      0.      0. 0.  0.                  lateral EFB (inactive) : lambda, flag
 0.  0.   0.    0.    0. 0.                                     # of non-zero C_i,  C_i (i=0,5), EFBS
 3.88494   0.  18.  50. 0. 0.                               DIPOLE #2 : ACN2, unused, B0, K, unused
 15. -1.                                                      entrance EFB
 4  .1455   2.2670  -.6395  1.1558  0. 0.  0.
 1.4896902673401404   0.    1.E6  -1.E6  1.E6  1.E6
 15. -1.                                                      exit EFB
 4  .1455   2.2670  -.6395  1.1558  0. 0.  0.
-1.4896902673401404   0.    1.E6  -1.E6  1.E6  1.E6
 0. 0.                                                        lateral EFB
 0  0.      0.      0.      0.      0. 0.  0.
 0.  0.   0.    0.    0. 0.
 5.89029  0.  -18.  50. 0. 0.                               DIPOLE #3 : ACN3, unused, B0, K, unused
 15. -1.                                        face 1        entrance EFB
 4  .1455   2.2670  -.6395  1.1558  0. 0.  0.
 0.5156620156177409   0.    1.E6  -1.E6  1.E6  1.E6
 15. -1.                                        face 2        exit EFB
 4  .1455   2.2670  -.6395  1.1558  0. 0.  0.
-0.5156620156177409   0.    1.E6  -1.E6  1.E6  1.E6
 0. 0.                                         face 3        lateral EFB
 0  0.      0.      0.      0.      0. 0.  0.
 0.  0.   0.    0.    0. 0.
  2  4.                                                     integration order, interpolation grid size
 1.                                                         integration step
 2   0.  0. 0. 0.
  'FAISCEAU'
'DRIFT     '
 156.
'REBELOTE'
31999 0.1 99                                                32000 turn tracking (in a single cell)
'END'
```

References

[1] A feasibility study of a NuFact in Japan, KEK report, Feb. 2001.

[2] Zgoubi users' guide, F. Méot and S. Valéro, CEA DAPNIA SEA-97-13 and FERMILAB-TM-2010 (1997).

[3] spes2, gsi

[4] Deflecting magnets, H.A. Enge, in *Focusing of charged particles*, Vol. 2, A. Septier ed., Academic Press, New-York and London (1967).